Wideband and low dispersion slow light by chirped photonic crystal coupled waveguide

Daisuke Mori and Toshihiko Baba

Yokohama National University, Department of Electrical and Computer Engineering
79-5 Tokiwadai, Hodogayaku, Yokohama 240-8501, Japan
baba@ynu.ac.jp

Abstract: Previously, we discussed an optical delay device consisting of a directional coupler of two different photonic crystal (PC) waveguides. It generates wideband and low dispersion slow light. However, it is easily degraded by a large reflection loss for a small imperfection of the coupling condition. In this paper, we propose and theoretically discuss a PC coupled waveguide, which allows more robust slow light with lower loss. For this device, unique photonic bands with a zero or negative group velocity at the inflection point can be designed by the structural tuning. Finite difference time domain simulation demonstrates the stopping and/or back and forth motion of an ultrashort optical pulse in the device combined with the chirped structure. For a signal bandwidth of 40 GHz, the average group index of the slow light will be 450, which gives a 1 ns delay for a device length of 670 μm. The theoretical total insertion loss at the device and input/output structures is as low as 0.11 dB.

OCIS codes: (230.3990) Microstructure devices; (230.3120) Integrated Optics Device

References and links

1. C. Li, Z. Dutton, C. H. Behroozi, and L. V. Hau, "Observation of coherent optical information storage in an atomic medium using halted light pulses," Nature **409**, 490-493 (2001).
2. R. D. Meade, A. Devenyi, J. D. Joannopoulos, O. L. Alerhand, D. A. Smith, and K. Kash, "Novel applications of photonic band gap materials: Low-loss bends and high Q cavities," Appl. Phys. Lett. **75**, 4753-4755 (1994).
3. A. Mekis, J. C. Chen, I. Kurland, S. Fan, P. R. Villeneuve, and J. D. Joannopoulos, "High transmission through sharp bends in photonic crystal waveguides," Phys. Rev. Lett. **77**, 3787-3790 (1996).
4. J. Yonekura, M. Ikeda, and T. Baba, "Analysis of finite 2-D photonic crystals of columns and lightwave devices using the scattering matrix method," J. Lightwave Technol. **17**, 1500-1508 (1999).
5. T. Baba, N. Fukaya, and J. Yonekura, "Observation of light propagation in photonic crystal optical waveguides with bends," Electron. Lett. **35**, 654-655 (1999); T. Baba, A. Motegi, T. Iwai, N. Fukaya, Y. Watanabe, and A. Sakai, "Light propagation characteristics of straight single line defect optical waveguides in a photonic crystal slab fabricated into a silicon-on-insulator substrate," IEEE J. Quantum Electron. **38**, 743-752 (2002).
6. M. Tokushima, H. Kosaka, A. Tomita, and H. Yamada, "Lightwave propagation through a 120 sharply bent single-line-defect photonic crystal waveguide," Appl. Phys. Lett. **76**, 952-954 (2000).
7. M. Lončar, D. Nedeljković, T. Doll, J. Vučković, and A. Scherer, "Waveguiding in planar photonic crystals," Appl. Phys. Lett. **77**, 1937-1939 (2000).
8. S. Noda, A. Chutinan, and M. Imada, "Trapping and emission of photons by a single defect in a photonic bandgap structure," Nature **407**, 608-610 (2000).
9. C. J. M. Smith, H. Benisty, S. Olivier, M. Rattier, C. Weisbuch, T. F. Krauss, R. M. De La Rue, R. Houdré, and U. Oesterle, "Low-loss channel waveguides with two-dimensional photonic crystal boundaries," Appl. Phys. Lett. **77**, 2813-2815 (2000).
10. M. Notomi, A. Shinya, K. Yamada, J. Takahashi, C. Takahashi, and I. Yokohama, "Singlemode transmission within photonic bandgap of width-varied single-line-defect photonic crystal waveguides on SOI substrates," Electron. Lett. **37**, 293-294 (2001); M. Notomi, A. Shinya, S. Mitsugi, E. Kuramochi, and H. -Y. Ryu, "Waveguides, resonators and their coupled elements in photonic crystal slabs," Opt. Express. **12**, 1551-1561 (2004), http://www.opticsexpress.org/abstract.cfm?URI=OPEX-12-8-1551
11. W. Bogaerts, V. Wiaux, D. Taillaert, S. Beckx, B. Luyssaert, P. Bienstman, and R. Baets, "Fabrication of photonic crystals in silicon-on-insulator using 248-nm deep UV lithography," IEEE J. Sel. Top. Quantum Electron. **8**, 928-934 (2002).

#8887 - $15.00 USD Received 23 September 2005; revised 2 November 2005; accepted 2 November 2005

12. S. J. McNab, N. Moll, and Y. A. Vlasov, "Ultra-low loss photonic integrated circuit with membrane-type photonic crystal waveguides," Opt. Express **11**, 2927-2939 (2003), http://www.opticsexpress.org/abstract.cfm?URI=OPEX-11-22-2927
13. Y. Sugimoto, Y. Tanaka, N. Ikeda, Y. Nakamura, K. Asakawa, and K. Inoue, "Low propagation loss of 0.76 dB/mm in GaAs-based single-line-defect two-dimensional photonic crystal slab waveguides up to 1 cm in length," Opt. Express **12**, 1090-1096 (2004), http://www.opticsexpress.org/abstract.cfm?URI=OPEX-12-6-1090
14. M. Notomi, K. Yamada, A. Shinya, J. Takahashi, C. Takahashi, and I. Yokohama, "Extremely large group-velocity dispersion of line defect waveguides in photonic crystal slabs," Phys. Rev. Lett. **87**, 253902 (2001).
15. K. Inoue, N. Kawai, Y. Sugimoto, N. Carlsson, N. Ikeda, and K. Asakawa, "Observation of small group velocity in two-dimensional AlGaAs-based photonic crystal slabs," Phys. Rev. B **65**, 121308 (2002).
16. T. Asano, K. Kiyota, D. Kumamoto, B-S. Song, and S. Noda, "Time-domain measurement of picosecond light-pulse propagation in a two-dimensional photonic crystal-slab waveguide," Appl. Phys. Lett. **84**, 4690-4692 (2004).
17. H. Gersen, T. J. Karle, R. J. P. Engelen, W. Bogaerts, J. P. Korterik, N. F. van Hulst, T. F. Krauss, and L. Kuipers, "Real-space observation of ultraslow light in photonic crystal waveguides," Phys. Rev. Lett. **94**, 073903 (2005).
18. M. D. Lukin, S. F. Yelin, and M. Fleischhauer, "Entanglement of atomic ensembles by trapping correlated photon states," Phys. Rev. Lett. **84**, 004232 (2000).
19. M. F. Yanik, W. Suh, Z. Wang, and S. Fan, "Stopping light in a waveguide with an all-optical analog of electromagnetically induced transparency," Phys. Rev. Lett. **93**, 233903 (2004).
20. T. Baba, D. Mori, K. Inoshita, and Y. Kuroki, "Light localization in line defect photonic crystal waveguides," IEEE J. Sel. Top. Quantum Electron. **10**, 484-491 (2004).
21. D. Mori and T. Baba, "Dispersion-controlled optical group delay device by chirped photonic crystal waveguides," Appl. Phys. Lett. **85**, 1101-1103 (2004).
22. M. L. Povinelli, S. G. Johnson, and J. D. Joannopoulos "Slow-light, band-edge waveguides for tunable time delays," Opt. Express. **13**, 7145-7159 (2005), http://www.opticsexpress.org/abstract.cfm?URI=OPEX-13-18-7145
23. A. Sakai, I. Katoh, D. Mori, T. Baba, and Y. Takiguchi, "Anomalous low group velocity and low dispersion in simple line defect photonic crystal waveguides," Proc. IEEE/LEOS Annual Meet., ThQ5 (2004).
24. A. Yu. Petrov and M. Eich, "Zero dispersion at small group velocities in photonic crystal waveguides," Appl. Phys. Lett. **85**, 4866-4868 (2004).
25. T. Ogawa, N. Yamamoto, Y. Watanabe, K. Komori, M. Itoh, and T. Yatagai, "Photonic crystal directional coupler switch with short switching length and wide band width," Proc. Fall Meet. of JSAP, 3p-ZC-14 (2004).
26. A. Sakai, G. Hara, and T. Baba, "Propagation characteristics of ultra-high Δ optical waveguide on silicon-on-insulator substrate," Jpn. J. Appl. Phys. **40**, L383-L385 (2001).
27. A. Sakai, T. Fukazawa, and T. Baba, "Low loss ultra-small branches in Si photonic wire waveguides," IEICE Trans. Electron. **E85-C**, 1033-1038 (2002).
28. D. Gerace and L. C. Andreani, "Disorder-induced losses in photonic crystal waveguides with line defects," Opt. Lett. **29**, 1897-1899 (2004).
29. S. Hughes, L. Ramunno, J. F. Young, and J. E. Sipe, "Extrinsic optical scattering loss in photonic crystal waveguides: role of fabrication disorder and photon group velocity," Phys. Rev. Lett. **94**, 033903 (2005).
30. S. G. Johnson, M. L. Povinelli, M. Soljacic, A. Karalis, S. Jacobs, and J. D. Joannopoulos, "Roughness losses and volume-current methods in photonic-crystal waveguides," Appl. Phys. B **81**, 283-293 (2005).
31. E. Mizuta, T. Ide, J. Hashimoto, K. Nozaki, T. Baba, T. Kise, K. Kiyota, and N. Yokouchi, "Characterization of photonic crystal waveguide for SOA operation," Proc. Pacific Rim Conf. Laser and Electro-Optics, CThE1-4 (2005).

1. Introduction

First-in-first-out (FIFO) optical buffer, which compress, stores and extracts optical signals on demand, is desired for sophisticate optical signal processing such as photonic routing. However, the tunable delay of optical pulses in a compact device of e.g. < 1 mm length is still a big challenge. Related with this topic, an anomalous low group velocity υ_g of light called *slow light* has attracted much attention recently. The phenomenon first studied for slow light was the electromagnetic induced transparency (EIT) [1]. It gives a huge group index $n_g \equiv c/\upsilon_g$ of light (c is the light velocity in vacuum) by the material dispersion. The photonic crystal (PC) waveguide [2-13], which has been developed as a platform of dense photonic circuits, also gives a huge n_g by the structural dispersion [14-17]. However, the slow light is generally restricted by the exclusive relation between the delay time and the frequency bandwidth. In addition, short optical pulses and high bitrate signals with a wide frequency spectrum are

#8887 - $15.00 USD Received 23 September 2005; revised 2 November 2005; accepted 2 November 2005

seriously distorted by the group velocity dispersion (GVD). To solve these problems, dynamic controls of the dispersion characteristics have been discussed for both EIT and PC [18, 19]. These methods stop optical pulses without changing their spatial envelope distribution. Therefore, they can be used for an optical memory in units of bits, but not for the FIFO buffer. Furthermore, an optical pulse with a full width at half maximum (FWHM) of 12.5 ps (40 Gbps signal) has a spatial full length of 2.5 mm for a medium index of 3.0. It is too long to store in a one bit memory without compression.

Previously, we proposed the chirped PC waveguide, in which some structural parameters are gradually changed so that photonic bands are smoothly shifted [20]. It allows a low υ_g and low GVD based on the principle shown in Fig. 1. Here, an ideal photonic band with the zero slope (zero υ_g condition) at the inflection point is prepared. The inflection point is sandwiched between negative and positive GVD band on the higher and lower frequency side, respectively. Let us consider the situation that the ideal band is shifted from the lower frequency side to the higher frequency side. Light first propagating with the negative GVD reaches the zero υ_g condition and is delayed. Due to the imperfect periodicity of the chirped structure, the light does not completely stop but soon moves forward with the positive GVD. In this process, the GVD is perfectly compensated, if the photonic band is symmetric against the inflection point. Such light propagation is obtained in a desired bandwidth by designing the chirped structure. We theoretically showed that such ideal band and light propagation are equivalently realized in a directional coupler consisting of two different chirped PC waveguides with opposite GVDs [21]. Also, the buttcoupling of chirped PC waveguides with opposite GVDs was theoretically discussed for the similar purpose [22]. However, these structures have a problem of large internal reflection loss at the directional coupling or the buttcoupling, unless very fine structures are realized. The simple structural tuning of the single line defect PC waveguide was also discussed to obtain the ideal band [23,24], but υ_g estimated is limited to $c/50$, which is not sufficient to obtain a nanosecond order delay in a device of, e.g., less than 1 mm length.

In this paper, we present a more ideal band obtained by a simpler structure, and theoretically demonstrate low loss slow light for an ultrashort optical pulse. We first describe the band engineering of the device which looks like a directional coupler but is used as a coupled waveguide. Next, we demonstrate the slow light and the unique light propagation, i.e., back and forth motion of the pulse, in finite difference time domain (FDTD) simulation. We discuss the relation between the slowdown factor given by the average group index and the available bandwidth. Finally, we show some candidate input/output (I/O) structures and the insertion loss, which are important for practical use.

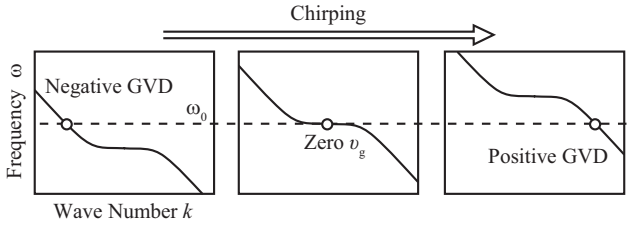

Fig. 1. Schematic of ideal band shifted by chirping against the frequency of incident light (dashed line).

2. Device and photonic band

The device structure and its photonic band are schematically shown in Fig. 2. Here, we make a premise to use the PC slab consisting of airholes in a high index membrane in future experiments, and consider its two-dimensional (2D) model with the effective index approximation in this theoretical work. We referred to the directional coupler consisting of two same kinds of PC waveguides [25]. In general, the directional coupler shows two photonic bands of coupled modes called even and odd modes. At the inter-waveguide spacing, the even mode has a higher intensity than the odd mode. Therefore, the increase in air filling

#8887 - $15.00 USD Received 23 September 2005; revised 2 November 2005; accepted 2 November 2005

factor at the spacing selectively pulls the even mode band up to the high frequency side, resulting in the ideal band shape with the zero υ_g condition at the inflection point. The target device operation is realized by regarding this device as a coupled waveguide with the selective input of the even mode.

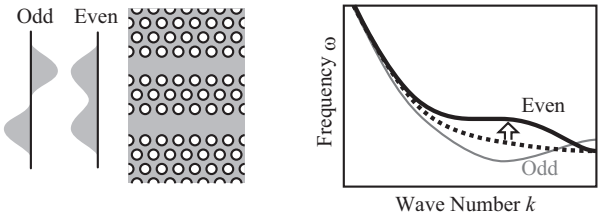

Fig. 2. Schematic of PC directional coupler with coupled mode profiles and corresponding bands.

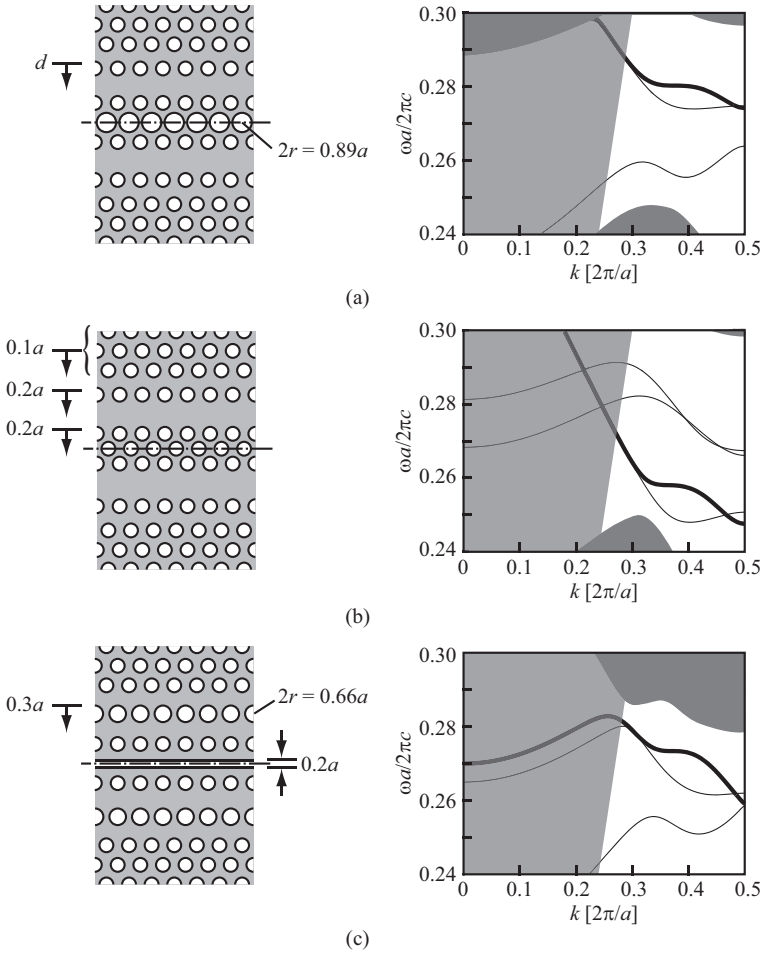

Fig. 3. Real structures of PC coupled waveguides and corresponding bands. Thick and thin lines indicate bands of the even mode and other modes, respectively. Light gray and dark gray regions show the light cone above the air light line and slab mode regions, respectively. For the band of (a), airhole shift *d* is set to be 0.25*a*.

#8887 - $15.00 USD Received 23 September 2005; revised 2 November 2005; accepted 2 November 2005

For the coupled waveguide, the diameter and position of airholes in the vicinity of two PC waveguides are used as design parameters. Figure 3 shows real structures and corresponding bands calculated by the plane wave expansion method. Here, we assumed the triangle lattice with the lattice constant a, a background index (equivalent modal index of the membrane) n of 2.963, and a basic airhole diameter $2r$ of $0.66a$ in (a) and $0.58a$ in (b) and (c). Along with the design concept mentioned above, the center airhole is enlarged in (a), the lateral inter-waveguide spacing is reduced in (b), and a linear airslit is inserted in (c). Moreover, the diameter and position of other holes are detuned for the further optimization of the band shape. In each structure, the almost ideal shape is observed for the even mode band indicated by the thick line. Since they are lying below the air light line, essential loss-less light propagation is expected when the device is fabricated into the PC slab. Particularly, (a) and (b) exhibit only the coupled mode bands in the target frequency range between the light line and the band-edge or slab mode region. Therefore, if only the even mode is excited at the input end of the device, the effective single mode propagation is obtained.

This device is used with the chirped structure. Later, we show the simulation of light propagation for the linear chirping of the background index n [21]. Ahead of that, let us check the index dependence of the band for the structure of Fig. 3(a). For n = 2.963 – 2.870, the band is shifted without changing its shape, as shown in Fig. 4; in the target frequency range, the change is only 0.03% of the center normalized frequency, which is difficult to evaluate

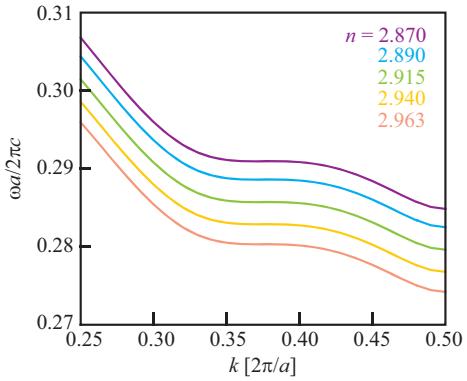

Fig. 4. Dependence of band for the structure of Fig. 3(a) on background index n, where d = $0.25a$ is assumed.

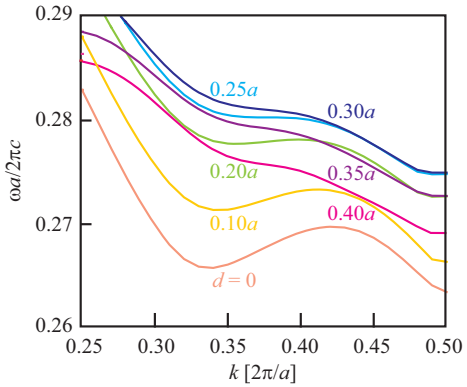

Fig. 5. Dependence of band for the structure of Fig. 3(a) on airhole shift d, where n = 2.963 is assumed.

#8887 - $15.00 USD Received 23 September 2005; revised 2 November 2005; accepted 2 November 2005

separately from the calculation error. This indicates that the change of υ_g of shifted bands at a particular frequency can be effectively evaluated from the frequency dependence of υ_g of a particular band. Figure 5 shows bands for the same structure with n = 2.963, where the airhole shift d is used as a parameter. At d = 0, the positive slope corresponding to a negative υ_g in the reduced zone scheme appears at the inflection point sandwiched by two extreme points. The slope gradually decreases with d, and becomes zero at d = 0.25a. At larger d, the slope becomes negative, which corresponds to a positive υ_g.

3. FDTD Analysis

In this section, we show the 2D FDTD simulation of light propagation for the index-chirped band. To model the actual PC slab device [5], we assumed a wavelength $\lambda \sim 1.55$ μm and a = 0.42 μm. The Yee cell size was as small as 10 nm (= a/42) to precisely model the hole diameter. The symmetric boundary condition was applied to the centerline, and a Gaussian pulse of 260 fs FWHM was excited with the even mode distribution to the surface normal component of the magnetic field H_z (TE polarization). The linear chirping of n was set from 2.963 to 2.870 for a chirped length of 50 μm.

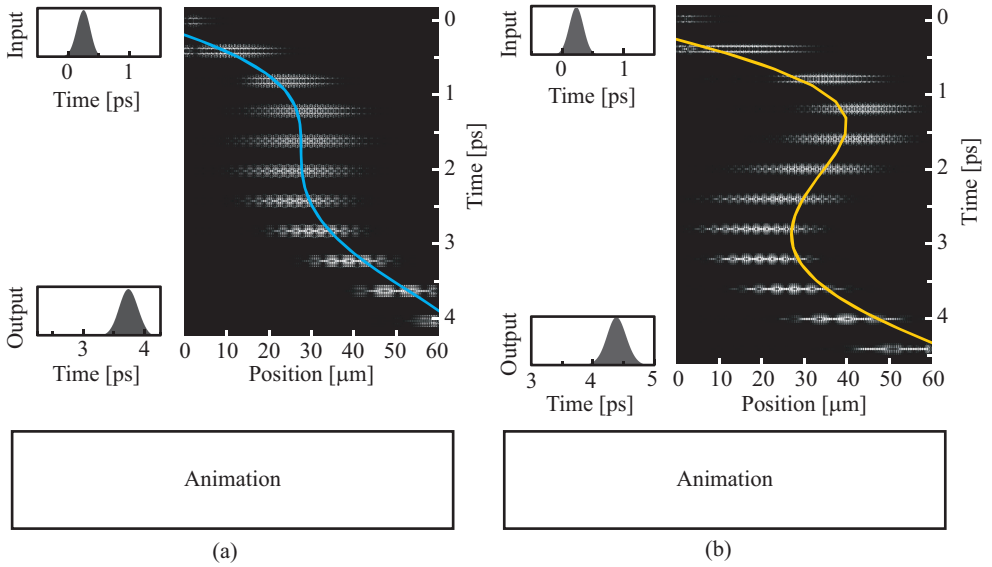

Fig. 6. Light intensity profile for each time frame and pulse waveforms of light power toward the right side. (a) and (b) are those for structures of Fig. 3(a) with d = 0.25a and 0.10a, respectively. Line in each figure shows corresponding photonic band. Animations show the light propagation (H_z field) for each structure, where red, yellow, green, light blue and dark blue show intensities from plus to minus.

The light intensity (H_z^2) profile at each time frame was calculated for structures of Fig. 3(a), as shown in Fig. 6(a) and (b), where excitation wavelengths were centered at 1.463 μm (a/λ = 0.287) and 1.505 μm (a/λ = 0.279), respectively. For the better understanding, their animations are also shown in attached multimedia files (a) and (b). In Fig. 6(a), the pulse coming from the left side reaches the zero υ_g condition and stops temporarily. It soon starts moving again and goes toward the right side. Referring to the discussion in the previous section, let us consider the frequency dependence of υ_g for the n = 2.963 band, instead of the band shift. Using the relation of $\upsilon_g = dx/dt = (dk/d\omega)^{-1}$, the band curve was overlaid on the intensity profiles in Fig. 6(a). It is clear that the pulse propagates along the band curve. The total delay time ΔT in the chirped region was 3.5 ps, and the average group velocity $\tilde{\upsilon}_g$ was

#8887 - $15.00 USD Received 23 September 2005; revised 2 November 2005; accepted 2 November 2005

c/20.9 (average group index $\tilde{n}_g$ = 20.9) although υ_g is much smaller than this value around the zero υ_g condition. Time waveforms of the pulse at the start and end points of the chirping are also shown in Fig. 6(a). The FWHM was expanded from Δt_s = 260 fs to Δt_e = 350 fs. It should be caused by the small asymmetry of the band shape. Still, the GVD compensation in this device is very effective for maintaining the pulse shape. The internal reflection was estimated from the power toward the left side at the start point to be as low as −28.2 dB. In Fig. 6(b), on the other hand, light toward the right side is reflected near the end point, reflected again near the start point, and finally passes through the device toward the right side. The overlaid band curve indicates that such light propagation arises from the band shape with two extreme points. Here, ΔT = 4.1 ps and $\tilde{\upsilon}_g = c/24.6$ ($\tilde{n}_g$ = 24.6). In this case, Δt_e was 330 fs. The reflection was estimated to be as low as −30.2 dB. The key parameter that determines this value is thought to be the slope of the chirping. If the device is lengthened and/or the chirp range is reduced, the reflection will be further reduced. Compared with previous devices, such a low reflection, which is ensured without any additional structures, is a big advantage of this device.

The back and forth motion in Fig. 6(b) can be explained by the schematic band diagram of Fig. 7 in the repeated zone scheme. Here, we again consider the frequency dependence of υ_g instead of the band shift. In general, the photonic band expresses the coupled state of the positive wavevector $\boldsymbol{k}_+$ and the negative wavevector $-\boldsymbol{k}_-$ through the lattice vector of $2\pi/a$ size, where $(\boldsymbol{k}_+ - \boldsymbol{k}_-) = 0$ only at the band-edge. The incident light at the start point A first reaches point B by the chirping. In this process, the light could take other eigen $\boldsymbol{k}$ vectors in the gray zone. However, the mutual coupling hardly occurs even in a chirped structure because of their large difference. (Although it is a qualitative expectation, calculated results in Fig. 6 well support it.) Since the band does not continue below point B, the light cannot go forward but must be reflected. Here, the reflected light is not coupled with the A'-B' band of the backward wave, even though $2\pi/a$ is operated. Thus, it is uniquely coupled with the B-C band with the negative υ_g. Similarly to this, it is coupled with the C-D band with the positive υ_g at point C, and finally reaches the end point D. This explanation can be also applied for Fig. 6(a) as the limit case that frequencies of B and C are equal. In this whole process, $\boldsymbol{k}$ (or $(\boldsymbol{k}_+ - \boldsymbol{k}_-)$ in other words) continuously decreases, resulting in the change of the lateral mode distribution from a profile with high intensity primarily in the waveguide regions to a profile with high intensity in the region between the waveguides, and the longitudinal envelope distribution from fastly oscillating to slowly oscillating.

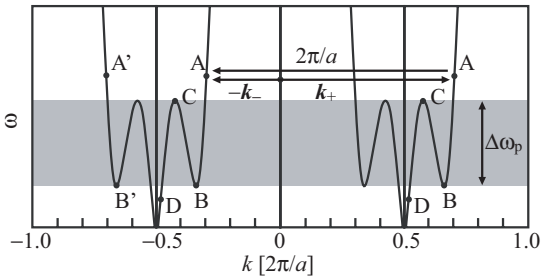

Fig. 7. Schematic band diagram in the repeated zone scheme for the explanation of back and forth motion in Fig. 6(b).

In Fig. 6, the spatial length of the pulse is kept almost constant throughout the propagation. But it is an accidental result caused by the assumed pulse width and chirped structure. Each frequency component of the pulse reaches the zero υ_g condition at a different position in the chirped structure. Therefore, the longitudinal envelope distribution of the stopped light has a profile related with the Fourier spectrum of the pulse, which is deformed by the time lag of

#8887 - $15.00 USD Received 23 September 2005; revised 2 November 2005; accepted 2 November 2005

light localization between different frequency components. Roughly speaking, the spatial pulse length in the chirped structure is inversely proportional to the spatial length of the initial pulse and the gradient of the chirping, although it is also changed by the time lag.

4. Average group velocity and delay-bandwidth product

We define the start and end points of the chirping to be at $x = 0$ and $x = \Delta L$, respectively. Then, ΔT is expressed as

$$\Delta T = \int_0^{\Delta L} \frac{dx}{\upsilon_g(x)} = \int_0^{\Delta L} \frac{n_g(x)}{c} dx \,. \tag{1}$$

The average group index $\tilde{n}_g$ is given by

$$\tilde{n}_g = \frac{c}{\tilde{\upsilon}_g} = \frac{c}{\Delta L / \Delta T} = \int_0^{\Delta L} n_g(x) dx \Big/ \Delta L \,. \tag{2}$$

By considering the frequency dependence of υ_g instead of the band shift, Eq. (2) is rewritten as

$$\tilde{n}_g \cong \int_{\omega_0}^{\omega_0+\Delta\omega} n_g(\omega) d\omega \Big/ \Delta\omega = \int_{\omega_0}^{\omega_0+\Delta\omega} c \frac{dk}{d\omega} d\omega \Big/ \Delta\omega = \int_{k_0}^{k_0+\Delta k} c dk \Big/ \Delta\omega = c \frac{\Delta k}{\Delta\omega} \tag{3}$$

where ω_0 and k_0 are the frequency and wavenumber at $x = 0$, respectively, and $\Delta\omega$ and Δk their change in the chirped structure, respectively. Equation (3) indicates that $\tilde{n}_g$ depends not on the fine band shape but on the linear slope from the start point to the end point. Therefore, $\tilde{n}_g$ can be enhanced by limiting $\Delta\omega$ to around the zero υ_g condition.

The signal bandwidth $\Delta\omega_s$ usable for slow light is not identical to $\Delta\omega$ but is restricted by the device principle and the used band shape. Let us assume that $\Delta\omega$ and $\Delta\omega_s$ are centered at the inflection point for bands of Fig. 5. If the small higher-order GVD is ignored, $\Delta\omega_s \le \Delta\omega/2$ becomes the minimum requirement for the GVD compensation when the band does not have extreme points at $d \ge 0.25a$. From Eq. (3), the product of the average group index and the normalized signal bandwidth (delay-bandwidth product) is

$$\tilde{n}_g \frac{\Delta\omega_s}{\omega} \le \tilde{n}_g \frac{\Delta\omega}{2\omega} = \frac{\Delta k}{2k} \,. \tag{4}$$

This equation indicates that, if $\tilde{n}_g$ is enhanced by limiting $\Delta\omega$, the delay-bandwidth product is reduced simultaneously with Δk. When the band has two extreme points at $d < 0.25a$, on the other hand, the overlapping of $\Delta\omega_s$ with the spectrum $\Delta\omega_p$ in Fig. 7 disturbs the complete back and forth motion of light. Therefore, $\Delta\omega_s$ must be evaluated by subtracting $\Delta\omega_p$ from $\Delta\omega$ such that $\Delta\omega_s \le (\Delta\omega - \Delta\omega_p)/2$. Then, the delay-bandwidth product is

$$\tilde{n}_g \frac{\Delta\omega_s}{\omega} \le \tilde{n}_g \frac{\Delta\omega - \Delta\omega_p}{2\omega} = \frac{\Delta k}{2k} \left(1 - \frac{\Delta\omega_p}{\Delta\omega} \right) \tag{5}$$

From Eqs. (3) – (5), upper limit values of $\tilde{n}_g$ and $\tilde{n}_g \Delta\omega_s/\omega$ for bands of Fig. 5 were calculated with $\Delta\omega_s/\omega$, as shown in Fig. 8. At $d = 0.25a$, which gives the zero υ_g condition at the inflection point, $\tilde{n}_g$ diverges to infinity at $\Delta\omega_s/\omega = 0$. For a bandwidth of 40 GHz at $\lambda = 1.55$ μm ($\Delta\omega_s/\omega = 2.1\times10^{-4}$), $\tilde{n}_g$ will be 450. When d is detuned from $0.25a$, $\tilde{n}_g$ and $\tilde{n}_g \Delta\omega_s/\omega$ become smaller in most cases. But when the signal bandwidth is wide, d slightly smaller than $0.25a$ gives larger values than those at $d = 0.25a$ due to the wide Δk and negligible $\Delta\omega_p$.

#8887 - $15.00 USD Received 23 September 2005; revised 2 November 2005; accepted 2 November 2005

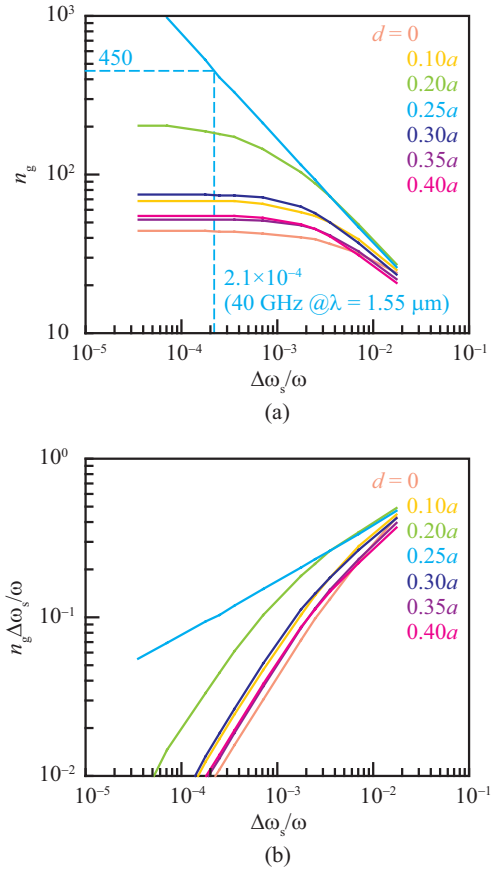

Fig. 8. Upper limit values of $\tilde{n}_g$ and $\tilde{n}_g\,\Delta\omega_s/\omega$ for bands of Fig. 5 calculated with $\Delta\omega_s/\omega$, where d is used as a parameter.

5. I/O structures

As explained in Section 2, this device needs the even mode input. A branch and a confluence are necessary at input and output ends, respectively, when the device is used with I/O waveguides. Here, the branch and the confluence must be optimized individually, because the modal profiles at the start and end points of the chirping are different, as shown in Section 3. We assumed the photonic wire waveguide [26] or the single line defect PC waveguide as I/O waveguides for the device structure of Fig. 3(a), and investigated low loss branches and confluences by the FDTD calculation for a = 0.42 μm at λ = 1.55 μm.

The branch and confluence optimized for photonic wire I/O waveguides are shown in Fig. 9. The index and width of the waveguide were assumed to be 2.963 and 0.5 μm, respectively. For the branch, the bend waveguide structure [27] of less than 0.1 dB excess loss was employed and connected to the device through tapers. We investigated some different tapers and found that the half elliptical taper allows the lowest connection loss of 0.44 dB. For the confluence, the lowest loss of 0.74 dB was estimated for the half circular funnel taper. Thus, the total insertion loss will be less than 1.3 dB.

Those optimized for PC I/O waveguides are shown in Fig. 10. The basic hole diameter of the waveguides, branch and confluence is expanded to 0.72a so that the waveguide band matches with the band of the device. For the PC branch, a loss of 0.08 dB was estimated when each branched waveguide was expanded to two line defects and the hole diameter at the edge

#8887 - $15.00 USD Received 23 September 2005; revised 2 November 2005; accepted 2 November 2005

of the branch was reduced to 0.48*a*. For the PC confluence, hole diameters at the edge of the confluence and at the corner were detuned to 0.48*a* and 0.80*a*, respectively, and a loss of 0.03 dB was estimated. Thus, the total insertion loss will be as low as 0.11 dB. Here, one has to care about the wavelength dependence of these PC components. The above parameters should be optimized for each operating wavelength of the device.

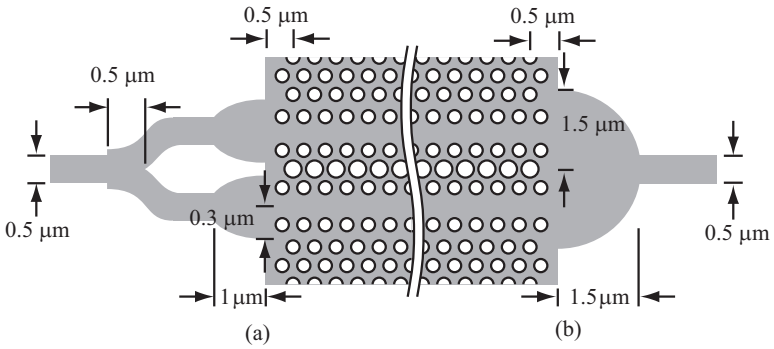

Fig. 9. I/O structure for the structure of Fig. 3(a) with photonic wire waveguides. (a) Half elliptical taper used with bend waveguide type branch. (b) Half circular funnel taper as a confluence.

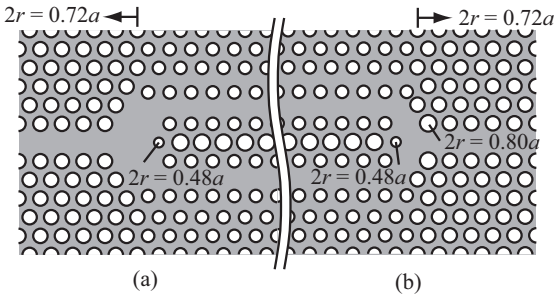

Fig. 10. I/O structure for the structure of Fig. 3(a) with PC single line defect waveguides. (a) Branch. (b) Confluence.

6. Conclusion

In this paper, we proposed and theoretically demonstrated the slow light device consisting of the PC coupled waveguide, which exhibits the zero group velocity at the inflection point of the photonic band. Using the chirped structure, an ultlashort optical pulse was stopped and delayed with maintaining its shape. By the slight detuning of parameters, the back and forth motion of the pulse was observed, which arises from the negative group velocity at the inflection point. The average group index was expected to be 450 for a signal bandwidth of 40 GHz. This means that a 1 ns delay is achieved in a 670-μm-long device. Moreover, a low insertion loss of 0.11 dB was expected when single line defect PC waveguides as well as the optimized branch and confluence were assumed as I/O structures.

Although all the calculations in this paper are 2D, we can expect the device operation in future experiments, because all the discussions were done for bands below the light line, and we know a rough correspondence between 2D and 3D bands. For the I/O structures, further optimization may be required in the experiment to suppress the out-of-plane radiation loss.

Since this device does not utilize any nonlinear effects and dynamic controls, it can be used as a FIFO buffer, which compresses, stores and extracts continuous signals without mutual interactions. Although only the fixed structures were discussed in this paper, the band shape will be flexibly changed by the local index control, and so a tunable delay will be available. The practical loss caused by the structural disordering is a significant issue for all

#8887 - $15.00 USD Received 23 September 2005; revised 2 November 2005; accepted 2 November 2005

the slow light researches. The investigation of the loss mechanism is very important [28-30], while the loss compensation by an external amplifier or an integrated PC amplifier [31] may be a practical solution for this issue.

This work was partly supported by The IT program and The 21st century COE program of MEXT, The Grant-In-Aid of JSPS, and The CREST Project of JST.

#8887 - $15.00 USD Received 23 September 2005; revised 2 November 2005; accepted 2 November 2005